# Theory of flux penetration into thin films with field-dependent critical current

J. McDonald and John R. Clem
*Ames Laboratory and Department of Physics and Astronomy, Iowa State University, Ames, Iowa 50011*
(Received 10 October 1995)

A theoretical analysis is presented for the critical state of an infinitely long type-II superconducting strip characterized by an arbitrary critical current density $J_c(B)$. An analytical framework is developed, and numerical solutions are presented for the quasistatic current-density and flux-density profiles, as well as the hysteretic magnetization curves. The field dependence of the critical current density significantly affects the shape of the magnetization curves.

## I. INTRODUCTION

There is currently considerable interest in thin-film and platelike superconductors. There have been numerous studies of single crystals of the high-temperature superconductors (HTSC), which are often in the form of platelets resembling thin-film rectangles or disks. Superconducting tapes of HTSC are under development for use in ac power transmission cables,[1,2] and epitaxial thin-film strips have been under investigation for passive microwave applications, such as filters for wireless communication.[3–5] There have been significant recent developments on the theory of the statics and dynamics of vortices in thin films.[6–13] This theoretical work has been motivated by advances in experimental techniques (magneto-optics,[9] scanning Hall probes,[14] Hall arrays,[10] scanning superconducting quantum interference device microscopes,[15] magnetic-force microscopy,[16] etc.) for determining magnetic-flux and current-density distributions in thin films.

In this paper we consider a thin-film strip and treat static or quasistatic magnetic-flux penetration and hysteresis characterized by a field-dependent critical current density $J_c(B)$. For this purpose, we employ a critical-state model.[6,7,17,18] In this model the magnetic flux penetrates into the superconductor in the form of vortices. This penetration occurs when the magnetic field at the sample surface exceeds the lower critical field $H_{c1}$. The density of vortices $n$ is assumed to be large enough ($n\lambda^2 \gg 1$, where $\lambda$ is the London penetration depth) that the vortices essentially form a continuum with average magnetic-flux density parallel to the vortices given by $B=n\phi_0$, where $\phi_0=hc/2e = 2.07\times10^{-7}$ G cm$^2$ is the superconducting flux quantum.[7]

The force per unit volume that tends to drive the vortices in from the surface is the Lorentz-force density $\mathbf{F}=\mathbf{J}\times\mathbf{B}$, where $\mathbf{J}=\nabla\times\mathbf{H}$. In the absence of a surface barrier, $\mathbf{B}$ and $\mathbf{H}$ satisfy the Maxwell boundary conditions at the sample surface (continuity of the normal component of $\mathbf{B}$ and the tangential component of $\mathbf{H}$). In critical-state models, it is typically assumed that, to good approximation, $\mathbf{B}=\mu_0\mathbf{H}$ in vortex-occupied regions. This is an excellent approximation when $B \gg \mu_0 H_{c1}$, which is often satisfied in HTSC. A quasistatic equilibrium obtains when the Lorentz-force density on the vortex array is balanced by the pinning-force density. The maximum pinning-force density is characterized by a critical current density $J_c$. When the magnitude of $\mathbf{J}$ exceeds $J_c$, the distribution of vortices, and hence $\mathbf{B}$, changes until the quasistatic equilibrium is restored.[7]

There is an important distinction in critical-state models between parallel and perpendicular geometries. As an example of the two geometries consider a circular cylinder of radius $R$ and length $L$ with an applied field parallel to $L$. If $L \gg R$, the parallel geometry is realized, while if $L \ll R$, the perpendicular geometry obtains. In the parallel geometry, the penetrating vortices are mostly parallel to the sample surface, while in the perpendicular geometry they are curved in the neighborhood of the sample surface because of the large demagnetizing effects.[6,7] This difference can be observed by examining the equation $\nabla\times\mathbf{B}=\mu_0\mathbf{J}$, where we have assumed $\mathbf{B}=\mu_0\mathbf{H}$. This equation can be written as $(\nabla B)\times\hat{\mathbf{B}}+B(\nabla\times\hat{\mathbf{B}})=\mu_0\mathbf{J}$, where $\hat{\mathbf{B}}=\mathbf{B}/B$.[6,20,21] The first term on the left-hand side depends on the spatial gradient of the flux density, while the second term depends on the curvature of the flux lines. In the parallel geometry the vortex lines curve very little and the gradient term dominates. This means that in the parallel geometry the Lorentz force stems mainly from gradients in magnetic pressure. In the perpendicular geometry, however, the magnetic-field lines bend around the sample and the tangential component has opposite signs on opposite sides of the sample. This leads to a large vortex curvature so that the second term on the left-hand side of the equation becomes dominant. Since the dominant terms are different in the two geometries, the structure of the critical state is also different.[6,7]

Recently many theoretical results have been reported for the critical state in thin films characterized by a field-independent $J_c$ (Bean model).[6,7,19,22,23] However, since it is observed experimentally that $J_c=J_c(B)$ in real materials, it is desirable to develop theoretical models that take this field dependence into account. This has been done for parallel geometry,[24–26] but relatively little has appeared in the literature for perpendicular geometry. Kuznetsov *et al.* estimated the effect of a field-dependent $J_c$ on the saturated magnetization of a disk in a large magnetic field.[28] Fedorov *et al.* treated the critical state in thin-film disks in a perpendicular applied field.[29] They were able to numerically calculate current-density and flux-density profiles, as well as hysteretic magnetization curves. Schuster *et al.*,[8] Brandt,[11,12] and Benkraouda and Clem[13] have shown that quasistatic results, for strips and disks, can be obtained numerically from dynamic

 

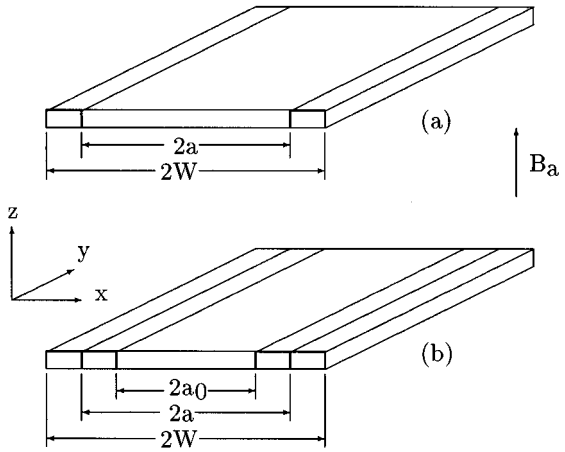


FIG. 1. Schematic of the strip and coordinate system. An external field $B_a$ is applied perpendicular to the strip. During initial flux penetration (a) the outer regions ($a<|x|<W$) carry a current density $J_y(x)=-(x/|x|)J_c(B_z(x))$ and contain a magnetic-flux density obeying Eq. (11). The central region ($|x|<a$) is perfectly screened [$B_z(x)=0$] and carries a current density given by Eq. (10). During field reversal (b) the outer regions ($a<|x|<W$) carry a current density $J_y(x)=(x/|x|)J_c(B_z(x))$ and contain a magnetic-flux density obeying Eq. (21). The inner regions ($a_0<|x|<a$) carry a current density given by Eq. (20) and contain the frozen-in magnetic-flux density from the previous flux front. The central region ($|x|<a_0$) is perfectly screened with a current density given by Eq. (20).

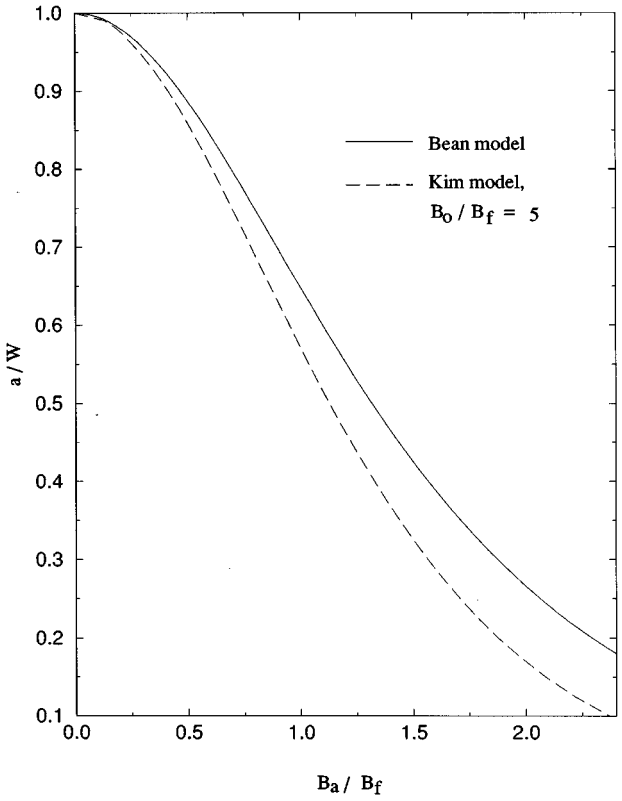


FIG. 2. Results for $a$ [see Fig. 1(a)] vs applied field $B_a$ calculated from Eqs. (11) and (12) during initial penetration. The solid curve corresponds to the Bean model, $J_c=J_{c0}$, while the dashed curve corresponds to the Kim model, $J_c=J_{c0}[B_o/(B_o+|B_z|)]$ with $B_o/B_f=5$ ($B_f=\mu_0 J_{c0}d/\pi$).

computations for $J_c=J_c(B)$ if the system is allowed to relax for an appropriate amount of time.

The purpose of this paper is to present a theoretical framework for the direct quasistatic treatment of the critical state in thin-film strips that are characterized by an arbitrary $J_c(B)$. The formalism presented is an extension of a method introduced by Mikheenko and Kuzovlev.[22] In their paper they treated a disk characterized by a constant $J_c$, but the method can be applied to the strip geometry and modified to include a field-dependent $J_c$.

## II. FLUX PENETRATION IN THE VIRGIN STATE

We begin by considering a thin, infinitely long superconducting strip of width $2W$ and thickness $d$. The strip is situated in the $x$-$y$ plane with its edges at $|x|=W$ and its long dimension parallel to the $y$ axis (cf. Fig. 1). A uniform field $B_a$ is applied perpendicular to the strip (parallel to the $z$ axis). We assume initially that $B_a$ is small enough that the strip is in the Meissner state. We can use the approximation of perfect screening if the width and thickness of the strip satisfy either $\lambda<d\ll W$ or $d<\lambda<\Lambda\ll W$, where $\lambda$ is the London penetration depth and $\Lambda=2\lambda^2/d$ is the two-dimensional screening length.[7,19,30] In this perfect-screening limit, the expressions for the current density (averaged over the thickness of the strip) and the perpendicular component of the flux density, in the plane of the strip, are well known.[6,7] Due to the symmetry of the problem, the current density has only a $y$ component. The expression for the current density, in SI units, is

$$J_y(x)=-\frac{2B_a}{\mu_0 d}\frac{x}{\sqrt{W^2-x^2}},\quad |x|<W, \tag{1}$$

where $\mu_0$ is the permeability of free space. If this current density is integrated with the Biot-Savart kernel, and the result is added to the applied field, the resulting flux density is

$$B_z(x)=\begin{cases} 0, & |x|<W, \\ B_a\dfrac{|x|}{\sqrt{x^2-W^2}}, & |x|>W. \end{cases} \tag{2}$$

These expressions are exact in the limit $d\to 0$, but in the case of finite $d$, $J_y$, and $B_z$ are understood to be averaged over the film thickness. In this case these expressions fail when the edges of the strip are approached too closely. The cutoff length for Eqs. (1) and (2) is $d$ if $d>\lambda$, or $\Lambda$ if $d<\lambda$.[7,19]

When $B_a$ becomes large enough [e.g., $B_a\gtrsim\sqrt{d/W}H_{c1}$, when $d<\lambda$] vortices will begin to penetrate from the edge.[7,27] These penetrating vortices will be either Abrikosov or Pearl vortices depending on whether $d>\lambda$ or $d<\lambda$. Dynamic equilibrium will occur when

$$J_y(x)=-\frac{x}{|x|}J_c(B_z(x)),\quad a<|x|<W. \tag{3}$$

The region $|x|<a$ remains perfectly screened [Fig. 1(a)].

As demonstrated by Mikheenko and Kuzovlev,[22] the expressions for the Meissner response can also be useful in the treatment of vortex penetration into a thin film. The key idea of their method is to express $J_y(x)$ and $B_z(x)$ for a flux-penetrated strip in terms of functions of the form of Eqs. (1) and (2),

$$J_y(x) = \begin{cases} \displaystyle\int_a^W dx' \left( \frac{-2B_a}{\mu_0 d} \frac{x}{\sqrt{x'^2 - x^2}} \right) G(x';B_a), & |x| < a, \\ \displaystyle\int_{|x|}^W dx' \left( \frac{-2B_a}{\mu_0 d} \frac{x}{\sqrt{x'^2 - x^2}} \right) G(x';B_a), & a < |x| < W, \end{cases} \tag{4}$$

$$B_z(x) = \begin{cases} \displaystyle\int_a^{|x|} dx' \left( B_a \frac{|x|}{\sqrt{x^2 - x'^2}} \right) G(x';B_a), & a < |x| < W, \\ \displaystyle\int_a^W dx' \left( B_a \frac{|x|}{\sqrt{x^2 - x'^2}} \right) G(x';B_a), & W < |x|, \end{cases} \tag{5}$$

where $G(x';B_a)$ is called the weight function. Once this function is determined, both $J_y(x)$ and $B_z(x)$ can be calculated. There is also a normalization equation for $G(x';B_a)$ that comes from requiring the flux density to vanish in the region $|x| < a$,

$$\int_a^W dx' G(x';B_a) = 1 . \tag{6}$$

Equation (6) yields the constitutive relation between $B_a$ and $a$.

To solve for $G(x';B_a)$, we invoke the force-balance requirement of Eq. (3),

$$\int_x^W dx' \left( \frac{-2B_a}{\mu_0 d} \frac{x}{\sqrt{x'^2 - x^2}} \right) G(x';B_a) = -J_c(B_z(x)), \quad a < x < W. \tag{7}$$

This Volterra equation for $G(x';B_a)$ can be inverted[31] to obtain

$$G(x;B_a) = -\frac{B_f}{B_a} \frac{d}{dx} \int_x^W \frac{dx'}{\sqrt{x'^2 - x^2}} \left( \frac{J_c(B_z(x'))}{J_{c0}} \right), \tag{8}$$

where the scaling field $B_f$ is defined by[7]

$$B_f = \frac{\mu_0 J_{c0} d}{\pi}, \tag{9}$$

and $J_{c0}$ is the zero-field critical current. Equation (8) can be inserted into Eqs. (4), (5), and (6). After integrating by parts, exercising care with the principal-value integrals, we obtain

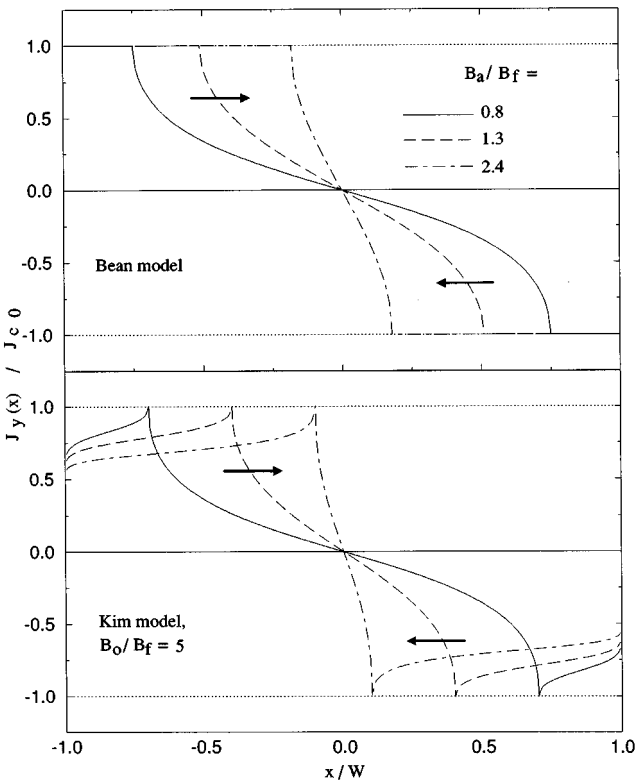


FIG. 3. Current-density profiles calculated from Eqs. (10), (11), and (12) for the Bean model (top) and Kim model (bottom) with $B_o/B_f = 5$ for $B_a/B_f = 0.8$ (solid), $B_a/B_f = 1.3$ (dashed), and $B_a/B_f = 2.4$ (dot-dashed). Bold arrows indicate the progression of the profiles as the applied field $B_a$ increases.

$$J_y(x) = \begin{cases} \displaystyle -\frac{2}{\pi} x \sqrt{a^2 - x^2} \int_a^W dx' \frac{J_c(B_z(x'))}{(x'^2 - x^2)\sqrt{x'^2 - a^2}}, & |x| < a, \\ \displaystyle -\frac{x}{|x|} J_c(B_z(x)), & a < |x| < W, \end{cases} \tag{10}$$

$$B_z(x) = B_f |x| \sqrt{x^2 - a^2} \int_a^W \frac{dx'}{(x^2 - x'^2)\sqrt{x'^2 - a^2}} \times \left( \frac{J_c(B_z(x'))}{J_{c0}} \right), \quad a < |x| \neq W, \tag{11}$$

$$B_a = B_f \int_a^W \frac{dx'}{\sqrt{x'^2 - a^2}} \left( \frac{J_c(B_z(x'))}{J_{c0}} \right). \tag{12}$$

If we set $J_c(B_z(x)) = J_{c0}$ in Eqs. (10), (11), and (12), we can recover the results obtained by Brandt and Indenbom[6] and Zeldov *et al.*[7]

If $J_c(B_z(x))$ is a function of $B_z(x)$, then Eq. (11) must be solved for $B_z(x)$ in the region $a < x < W$. In general this is a nonlinear Fredholm equation, which must be solved numerically. Once this has been done, $J_y(x)$, $B_z(|x| > W)$, and $B_a$ can be calculated from Eqs. (10), (11), and (12), respectively. $\mathbf{B}(x,z)$ can also be calculated from

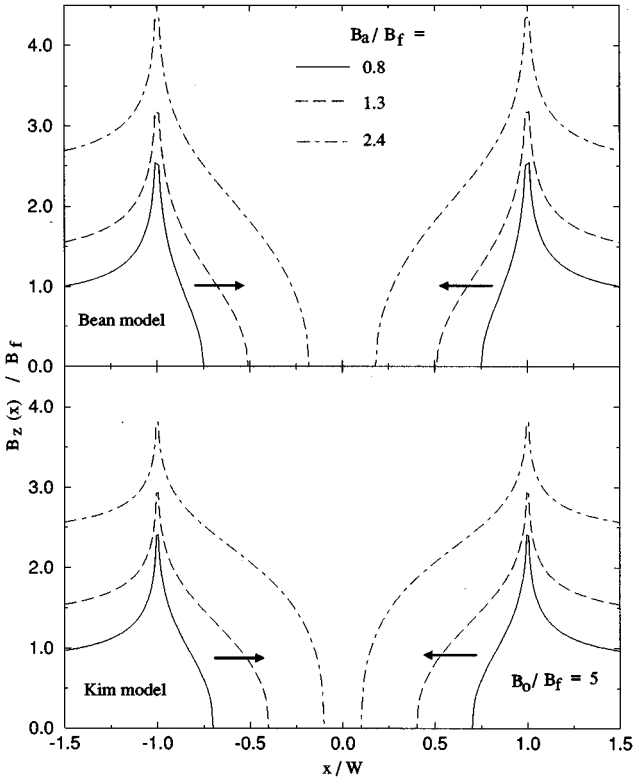


FIG. 4. Flux-density profiles calculated from Eqs. (11) and (12) for the Bean model (top) and Kim model (bottom) with $B_o/B_f=5$ for $B_a/B_f=0.8$ (solid), $B_a/B_f=1.3$ (dashed), and $B_a/B_f=2.4$ (dot-dashed). Bold arrows indicate the progression of the profiles as the applied field $B_a$ increases.

$$\mathbf{B}(x,z)=\frac{\mu_0 d}{2\pi}\int_{-W}^{W}dx' J_y(x')\frac{(x'-x)\hat{z}+z\hat{x}}{(x'-x)^2+z^2}. \qquad (13)$$

Until now, we have not assumed anything about the form of $J_c(B_z(x))$. As a specific example we can choose

$$\frac{J_c(B_z(x))}{J_{c0}}=\frac{B_o}{B_o+|B_z(x)|}$$

(Kim model),[32] where $B_o$ is a constant field that characterizes the degree of field dependence [$J_y(x)=J_{c0}/2$ when $B_z(x)=B_o$]. The numerical results for $B_o/B_f=5$ are shown in Figs. 2–4. The field dependence of $J_c$ leads to a larger amount of penetration in a given applied field (smaller $a$ for a given $B_a$), as demonstrated in Fig. 2. Figure 3 shows that the field dependence of $J_c$ causes cusplike peaks in $|J_y(x)|$ at the values of $x$ where $B_z(x)=0$, and a strong suppression of $|J_y(x)|$ at the edges where $B_z(x)$ is large. It should be noted that the cusplike features in Fig. 3, and the apparent divergence of $B_z(|x|=W)$ in Fig. 4, are rounded on the length scale of $d$, if $\lambda<d$, or $\Lambda$, if $d<\lambda$. Figure 4 demonstrates that the shapes of the $B_z(x)$ versus $x$ curves are qualitatively very similar for both the field-independent and field-dependent $J_c$ cases, the main difference being the greater degree of penetration in the field-dependent case.

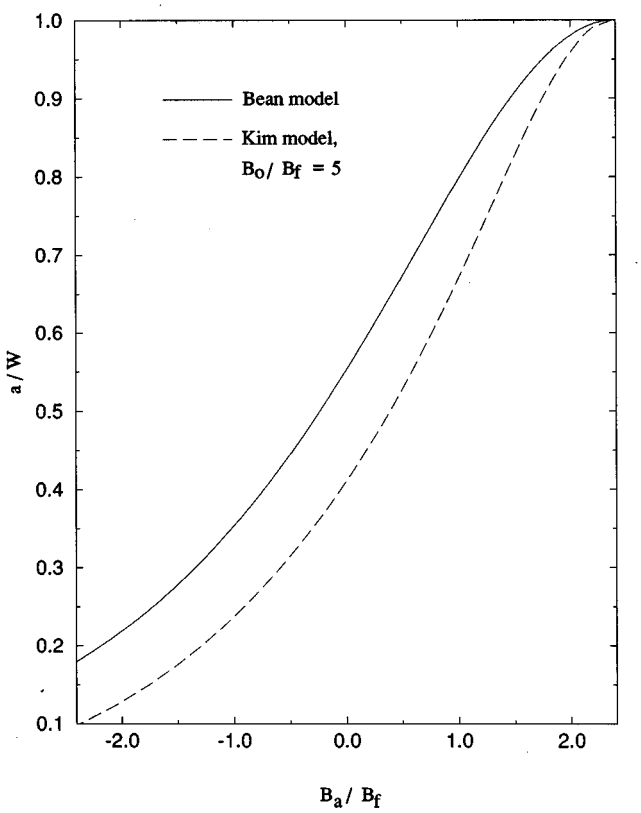


FIG. 5. Results for $a$ [see Fig. 1(b)] vs applied field $B_a$ during field reversal from $B_a=B_{a0}=2.4B_f$ to $B_a=-B_{a0}$, calculated from Eqs. (21) and (22). The solid curve corresponds to the Bean model, while the dashed curve corresponds to the Kim model with $B_o/B_f=5$.

## III. FLUX CHANGES UPON FIELD REVERSAL

We now consider the case of decreasing the applied field from an initial value $B_{a0}$ to some lower value $B_a=B_{a0}-\Delta B_a$, where $\Delta B_a\leqslant 2B_{a0}$. We assume that when $B_a=B_{a0}$ the strip is penetrated with positive flux in the regions $a_0<|x|<W$, and is completely screened in the region $|x|<a_0$. After the field is decreased, the flux density changes in the outer regions ($a<|x|<W$) but is unchanged in the inner regions ($a_0<|x|<a$). The central region ($|x|<a_0$) remains free of flux [Fig. 1(b)]. The current density in the outer regions is given by Eq. (3) without the negative sign. Since we are considering a thin film, the current is altered throughout the sample.[7]

As in the previous section, we express $J_y(x)$ and $B_z(x)$ in terms of a new weight function $G(x';B_a)$ as follows:

$$J_y(x)$$

$$=\begin{cases}\displaystyle\int_{a_0}^{W}dx'\left(\frac{-2B_a}{\mu_0 d}\frac{x}{\sqrt{x'^2-x^2}}\right)G(x';B_a), & |x|<a_0,\\ \displaystyle\int_{|x|}^{W}dx'\left(\frac{-2B_a}{\mu_0 d}\frac{x}{\sqrt{x'^2-x^2}}\right)G(x';B_a), & a_0<|x|<W,\end{cases} \qquad (14)$$

$$B_z(x)=\begin{cases}\displaystyle\int_{a_0}^{|x|}dx'\left(B_a\frac{|x|}{\sqrt{x^2-x'^2}}\right)G(x';B_a), & a_0<|x|<W,\\ \displaystyle\int_{a_0}^{W}dx'\left(B_a\frac{|x|}{\sqrt{x^2-x'^2}}\right)G(x';B_a), & W<|x|.\end{cases}\tag{15}$$

The vanishing of the flux density for $|x|<a_0$ leads to a normalization equation for $G(x;B_a)$

$$\int_{a_0}^{W}dx'\,G(x';B_a)=1\,.\tag{16}$$

As in the previous section, this equation yields the constitutive relation between $B_a$ and $a$.

To solve for $G(x;B_a)$, however, we require two equations. The first comes from the critical-state model [cf. Eq. (3)],

$$\int_{x}^{W}dx'\left(\frac{-2B_a}{\mu_0 d}\frac{x}{\sqrt{x'^2-x^2}}\right)G(x';B_a)=J_c(B_z(x)),\qquad a<x<W,\tag{17}$$

and the second comes from our knowledge of the flux density in the inner region $a_0<x<a$,

$$\int_{a_0}^{x}dx'\left(B_a\frac{x}{\sqrt{x^2-x'^2}}\right)G(x';B_a)=B_z(x),\qquad a_0<x<a.\tag{18}$$

Both of these Volterra equations can be inverted,[31]

$$G(x;B_a)=\begin{cases}\dfrac{2}{\pi}\dfrac{d}{dx}\displaystyle\int_{a_0}^{x}\frac{dx'}{\sqrt{x^2-x'^2}}\left(\frac{B_z(x')}{B_f}\right), & a_0<x<a,\\ \dfrac{B_f}{B_a}\dfrac{d}{dx}\displaystyle\int_{x}^{W}\frac{dx'}{\sqrt{x'^2-x^2}}\left(\frac{J_c(B_z(x'))}{J_{c0}}\right), & a<x<W.\end{cases}\tag{19}$$

If we insert Eq. (19) into Eqs. (15), (16), and (17) and integrate by parts, we obtain

$$J_y(x)=\begin{cases}\dfrac{2}{\pi}x\sqrt{a^2-x^2}\left[\displaystyle\int_a^W dx'\frac{J_c(B_z(x'))}{(x'^2-x^2)\sqrt{x'^2-a^2}}-\frac{2}{\pi}J_{c0}\int_{a_0}^{a}\frac{dx'}{(x'^2-x^2)\sqrt{a^2-x'^2}}\left(\frac{B_z(x')}{B_f}\right)\right], & |x|<a,\\ \dfrac{x}{|x|}J_c(B_z(x)), & a<|x|<W,\end{cases}\tag{20}$$

$$B_z(x)=|x|\sqrt{x^2-a^2}\left[-B_f\int_a^W\frac{dx'}{(x^2-x'^2)\sqrt{x'^2-a^2}}\left(\frac{J_c(B_z(x'))}{J_{c0}}\right)+\frac{2}{\pi}\int_{a_0}^{a}dx'\frac{B_z(x')}{(x^2-x'^2)\sqrt{a^2-x'^2}}\right],\qquad a<|x|\neq W,\tag{21}$$

$$B_a=-B_f\int_a^W\frac{dx'}{\sqrt{x'^2-a^2}}\left(\frac{J_c(B_z(x'))}{J_{c0}}\right)+\frac{2}{\pi}\int_{a_0}^{a}dx'\frac{B_z(x')}{\sqrt{a^2-x'^2}}.\tag{22}$$

When $J_c(B_z(x))=J_{c0}$, Eqs. (20), (21), and (22) yield the results of Brandt and Indenbom[6] and Zeldov *et al.*[7] If $J_c(B_z(x))$ is a function of $B_z(x)$, then Eq. (21) must be solved numerically for $B_z(x)$ in the regions $a<|x|<W$. Then $J_y(x)$, $B_z(|x|>W)$, $B_a$, and $\mathbf{B}(x,z)$ can be calculated from Eqs. (20), (21), (22), and (13), respectively. As a specific example, we choose the same functional form for $J_c(B_z(x))$ as in the previous section. The numerical results for $B_a$ decreasing from its initial value, $B_{a0}=2.4B_f$, to its final value, $-B_{a0}$, are shown for $B_o/B_f=5$ in Figs. 5–7. Figure 6 demonstrates that the $J_y(x)$ versus $x$ curves, for the field-dependent $J_c$ case, have cusplike peaks at $|x|=a_0$, sharp elbowlike features at $|x|=a$, extrema at the values of $x$ for which $B_z(x)=0$, and a suppression of $|J_y(x)|$ at the edge. The sharp features in Fig. 6, and the apparent divergence of $B_z(|x|=W)$ in Fig. 7, are rounded on the length scale $d$, if $\lambda<d$, or $\Lambda$, if $d<\lambda$. The $B_z(x)$ versus $x$ curves in Fig. 7 are qualitatively similar for both the field-independent and field-dependent $J_c$ cases, but differ in the amount of penetration because it is easier for vortices to penetrate in the field-dependent case because of the suppression of the critical current.

## IV. MAGNETIZATION AND HYSTERESIS

In the previous sections we have established the machinery for calculating critical-state current-density and flux-density profiles for a thin strip. We are now in a position to calculate hysteretic magnetization curves for a strip placed in an alternating applied field. The magnetization per unit volume is given by[6,7]

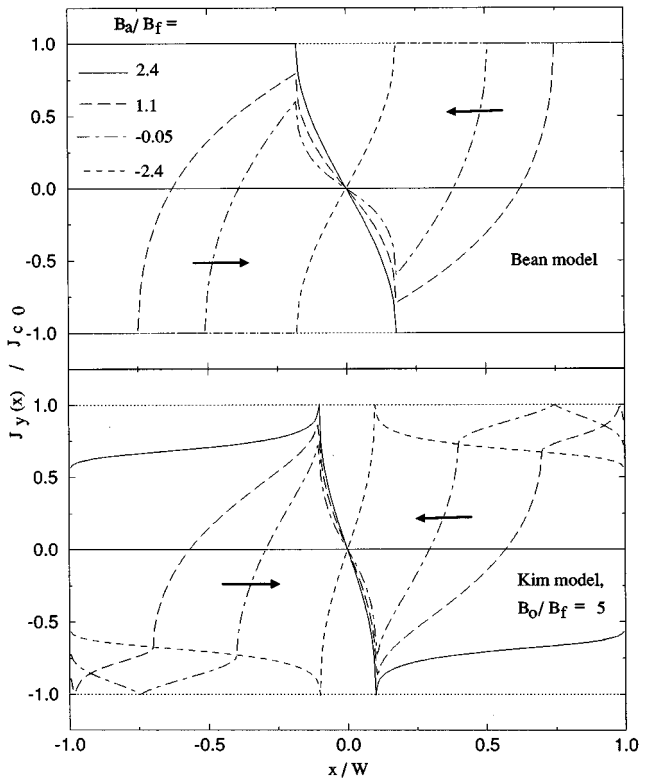


FIG. 6. Decreasing-field current-density profiles calculated from Eqs. (20), (21), and (22) for the Bean model (top) and the Kim model (bottom) with $B_o/B_f=5$ for $B_a/B_f=B_{a0}/B_f=2.4$ (solid), $B_a/B_f=1.1$ (long dashed), $B_a/B_f=-0.05$ (dot-dashed), and $B_a/B_f=-2.4$ (short dashed). Bold arrows indicate the progression of the profiles as the applied field $B_a$ increases.

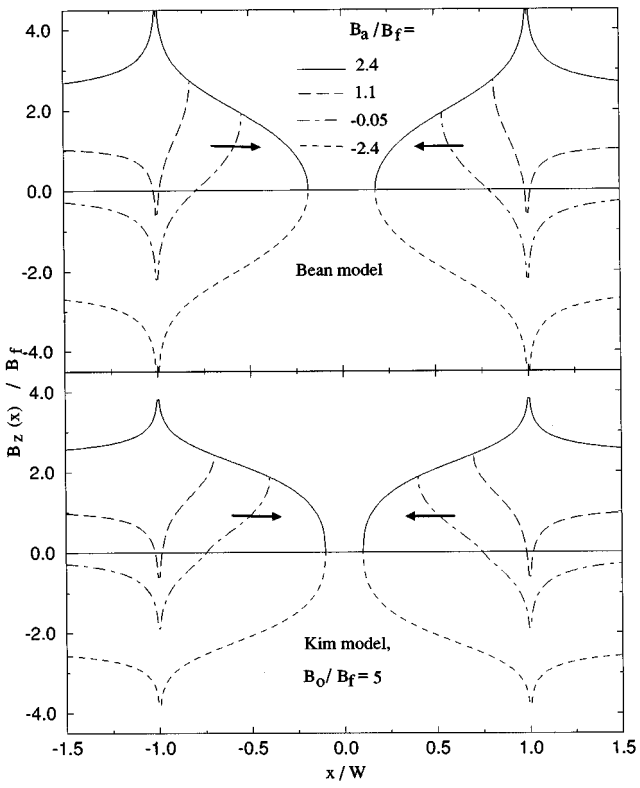


FIG. 7. Decreasing-field flux-density profiles calculated from Eqs. (21) and (22) for the Bean model (top) and the Kim model (bottom) with $B_o/B_f=5$ for $B_a/B_f=B_{a0}/B_f=2.4$ (solid), $B_a/B_f=1.1$ (long dashed), $B_a/B_f=-0.05$ (dot-dashed), and $B_a/B_f=-2.4$ (short dashed). Bold arrows indicate the progression of the profiles as the applied field $B_a$ increases.

$$M_z=\frac{1}{2W}\int_{-W}^{W}dx\ xJ_y(x). \tag{23}$$

The maximum possible value of $M_z$ occurs when the strip is saturated with the zero-field critical current density,

$$M_0=\frac{J_{c0}W}{2}. \tag{24}$$

This can only occur for a field-independent $J_c$.

We assume that initially $B_a=0$ and that the strip is in the virgin state. $B_a$ is then increased by a small amount so that there is a positive flux in the regions $a<|x|<W$ and no flux in the region $|x|<a$ [Fig. 1(a)]. Using the formalism of Sec. II we can calculate $J_y(x)$ and $B_z(x)$, and hence $M_z$ and $B_a$. We continue this process until the regions $a_0<|x|<W$ are occupied with positive flux. At this stage $B_a=B_{a0}$. $B_a$ is then decreased by a small amount so that the flux density changes in the regions $a<|x|<W$. There is a frozen-in flux in the regions $a_0<|x|<a$, and the region $|x|<a_0$ remains perfectly screened [Fig. 1(b)]. The results of Sec. III can be employed to calculate $J_y(x)$ and $B_z(x)$. $M_z$ and $B_a$ are then computed. This process is continued until the regions $a_0<|x|<W$ are filled with negative flux ($B_a=-B_{a0}$). $B_a$ is then increased to $B_{a0}$ in small increments and $M_z$ and $B_a$ are again determined at each step. The resulting graph of $M_z$ versus $B_a$ is the hysteretic magnetization curve or hysteresis loop.

Examples of these curves are shown in Fig. 8. For the case of a weakly field-dependent $J_c$ [Fig. 8(a)] the curves become flattened on the top and bottom and $M_z$ tends to $M_0$ as saturation is approached (large $B_{a0}$). This is characteristic of the field-independent $J_c$ limit.[6,19] As $J_c$ becomes more field-dependent [Figs. 8(b) and 8(c)] the curves start to develop extrema near $B_a=0$ and close up near the ends. This is more characteristic of experimental hysteresis loops.

## V. SUMMARY

We have presented a method for the treatment of the critical state in a type-II superconducting thin-film strip, characterized by an arbitrary $J_c(B)$, in a uniform, time-varying applied field. We have shown how this method can be used to calculate quasistatic current-density and flux-density profiles, as well as magnetization curves for a strip in an alternating field.

These results should have important applications in the interpretation of experimental data. It is now possible to map out flux-density and current-density profiles in thin films.[9,14] From these measurements the field dependence of $J_c$ can be determined. Once this is known, the flux-density and current-density profiles can be calculated and compared with the

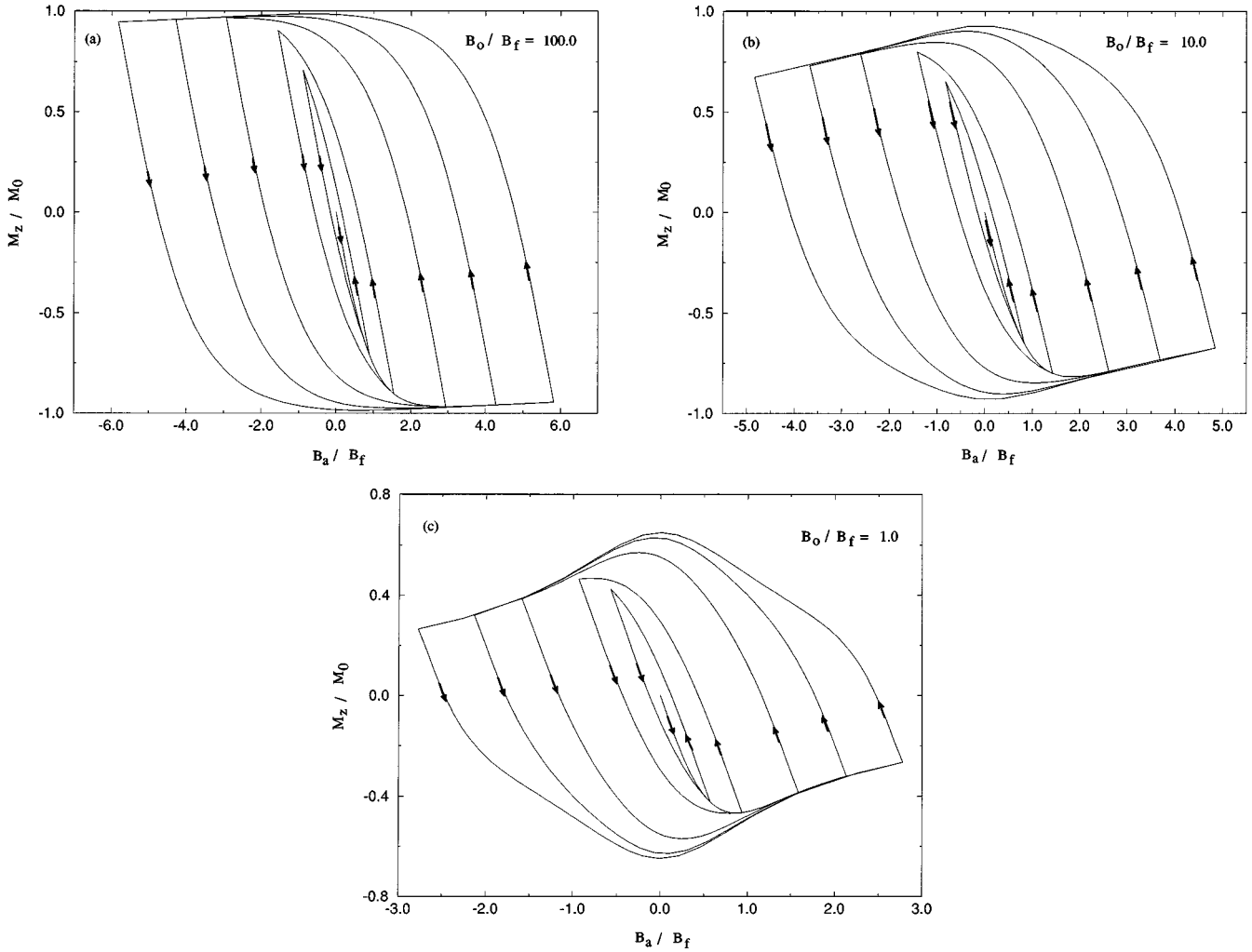


FIG. 8. Hysteretic magnetization curves, $M_z/M_0$ vs $B_a/B_f$, calculated as described in the text for the Kim model with (a) $B_o/B_f=100.0$, (b) $B_o/B_f=10.0$, and (c) $B_o/B_f=1.0$.

measured profiles. The method should also find applications in the interpretation of ac-susceptibility measurements. In analogy with samples in the parallel geometry, one would expect a field-dependent $J_c$ to lead to the generation of even harmonics in the ac-susceptibility response of a sample subjected to a perpendicular dc field. These even harmonics vanish in the field-independent case.[33] The method should also find use in the interpretation of measurements of magnetization hysteresis loops and irreversible magnetization. It was demonstrated in Sec. IV that the field dependence of $J_c$ has a profound impact on the shape of the magnetization curves.

Extension of the method to treat the case of a strip carrying a transport current is straightforward. The effect of a field-dependent $J_c$ on the ac losses can then be studied and compared with the well-known result for the field-independent case ($P_{\rm loss}\sim I^4$).[18] This will be the subject of a future paper.

## ACKNOWLEDGMENTS

We thank M. Benkrouda, E. H. Brandt, M. McElfresh, T. Pe, A. Sanchez, and E. Zeldov for stimulating discussions. Ames Laboratory is operated for the U.S. Department of Energy by Iowa State University under Contract No. W-7105-Eng-82.

[1] A. M. Campbell, IEEE Trans. Appl. Supercond. **5**, 687 (1995).
[2] S. Fleshler, L. T. Cronis, G. E. Conway, A. P. Malozemoff, T. Pe, J. McDonald, J. R. Clem, G. Vellego, and P. Metra, Appl. Phys. Lett. **67**, 3189 (1995).
[3] D. E. Oates, P. P. Nguyen, G. Dresselhaus, M. S. Dresselhaus, G. Koren, and E. Polturak, J. Supercond. **8**, 725 (1995).
[4] G. B. Lubkin, Phys. Today **40** (3), 20 (1995).
[5] Z.-Y. Shen, *High-Temperature Superconducting Microwave Circuits* (Artech, Boston, 1994).
[6] E. H. Brandt and M. Indenbom, Phys. Rev. B **48**, 12 893 (1993).
[7] E. Zeldov, J. R. Clem, M. McElfresh, and M. Darwin, Phys. Rev. B **49**, 9802 (1994).
[8] T. Schuster, H. Kuhn, E. H. Brandt, M. Indenbom, M. R. Koblishka, and M. Konczykowski, Phys. Rev. B **50**, 16 684 (1994).

[9] T. Schuster, M. V. Indenbom, H. Kuhn, E. H. Brandt, and M. Konczykowski, Phys. Rev. Lett. **73**, 1424 (1994).
[10] E. Zeldov, A. I. Larkin, V. B. Geshkenbein, M. Konczykowski, D. Majer, B. Khaykovich, V. M. Vinokur, and H. Shtrikman, Phys. Rev. Lett. **73**, 1428 (1994).
[11] E. H. Brandt, Physica C **235-240**, 2939 (1994).
[12] E. H. Brandt, Rep. Prog. Phys. **58**, 1465 (1995).
[13] M. Benkraouda and J. R. Clem, Phys. Rev. B **53**, 5716 (1996).
[14] W. Xing, B. Heinrich, H. Zhou, A. A. Fife, and A. R. Cragg, J. Appl. Phys. **76**, 4244 (1994).
[15] C. C. Tsuei, J. R. Kirtley, C. C. Chi, L. S. Yu-Jahnes, A. Gupta, T. Shaw, J. Z. Sun, and M. B. Ketchen, Phys. Rev. Lett. **73**, 593 (1994).
[16] A. Moser, H. J. Hug, I. Parashikov, B. Stiefel, O. Fritz, H. Thomas, A. Baratoff, H.-J. Guntherödt, and P. Chaudhari, Phys. Rev. Lett. **74**, 1847 (1995).
[17] C. P. Bean, Phys. Rev. Lett. **8**, 250 (1962).
[18] W. T. Norris, J. Phys. D **3**, 489 (1970).
[19] J. R. Clem and A. Sanchez, Phys. Rev. B **50**, 9355 (1994).
[20] J. R. Clem, in *Proceedings of the ICTPS'90 International Conference on Transport Properties of Superconductors*, edited by R. Nicolsky (World Scientifice, Singapore, 1990), p. 64.
[21] J. R. Clem, in *Proceedings of the 7th International Workshop on Critical Currents in Superconductors*, edited by H. W. Weber (World Scientific, Singapore, 1994), p. 117.
[22] P. N. Mikheenko and Y. E. Kuzovlev, Physica C **204**, 229 (1993).
[23] J. Zhu, J. Mester, J. Lockhart, and J. Turneaure, Physica C **212**, 216 (1993).
[24] J. R. Clem, J. Appl. Phys. **50**, 3518 (1979).
[25] D.-X. Chen and R. B. Goldfarb, J. Appl. Phys. **66**, 2489 (1989).
[26] H. Ikuta, K. Kishio, and K. Kitazawa, J. Appl. Phys. **76**, 4776 (1994).
[27] V. N. Trofimov, A. V. Kuznetsov, P. V. Lepeschkin, K. A. Bolschinskov, A. A. Ivanov, and A. A. Mikhailov, Physica C **183**, 135 (1991).
[28] A. V. Kuznetsov, A. A. Ivanov, D. V. Eremenko, and V. N. Trofimov, Phys. Rev. B **52**, 9637 (1995).
[29] Y. A. Fedorov, V. G. Fleisher, and M. G. Semenchenko, Physica C **217**, 63 (1993).
[30] J. Pearl, Appl. Phys. Lett. **5**, 65 (1964).
[31] P. Linz, *Analytical and Numerical Methods for Volterra Equations* (S.I.A.M, Philadelphia, 1985), p. 74.
[32] Y. B. Kim, C. F. Hempstead, and A. R. Strand, Phys. Rev. Lett. **9**, 306 (1962).
[33] Q. Y. Chen, in *Magnetic Susceptibility of Superconductors and Other Spin Systems*, edited by R. A. Hein *et al.* (Plenum, New York, 1991), p. 81.